OPTIMIZATION OF THE FLUE GAS-FLOW CONTROLLING DEVICES OF THE ELECTROSTATIC PRECIPITATOR OF UNIT A4 IN TPP "NIKOLA TESLA"

Zoran J. MARKOVIĆ**, Milić D. ERIĆ, Predrag Lj. STEFANOVIĆ, Rastko D. JOVANOVIĆ, and Ivan M. LAZOVIĆ

"VINČA" Institute of Nuclear Sciences, National Institute of the Republic of Serbia, University of Belgrade, Vinča, Belgrade, Serbia

Original scientific paper
https://doi.org/10.2298/TSCI220903024M

Homogeneity of the flue gas-flow through the chamber of an electrostatic precipitator is one of the basic influencing parameter on dedusting efficiency. This paper presents results of a multiobjective optimization study of the flue gas controlling devices of electrostatic precipitator of 324 MWe lignite fired Unit A4 of TPP "Nikola Tesla" in Serbia. The aim was to achieve better flow homogeneity in the cross-section of the precipitator compared to the original design. Additional constraints were to maintain the minimum as possible overall weight of the proposed design as well as pressure drop through the precipitator. Numerical simulations based on CFD were used to investigate dependence of the velocity distribution in the ducts and precipitator's chamber with respect to the geometrical parameters of tested concepts of turning blades. A series of 22 detailed full-scale numerical models of the precipitator with different concepts of turning vanes designs were developed. Assessment of the flow field uniformity for each tested design was performed based on the analysis of several homogeneity parameters calculated for selected vertical cross-sections of the precipitator. After the reconstruction according to optimized design, results of measurements confirmed significant improvements of the velocity distribution in the vertical cross-sections of the precipitator, increase of dedusting efficiency and reduction of PM emission.

Key words: *efficiency of electrostatic precipitator, flow uniformity, gas velocity measurements, CFD*

Introduction

The electrostatic precipitator (ESP) dedusting performance significantly depends on the flue gas velocity distribution and turbulence level inside of ESP chamber [1]. If local gas velocities are too high, the aerodynamic forces upon the particles can overwhelm the electrostatic forces. In the case of too low local velocities collecting surface is not being adequately utilized leading to degradation in collection efficiency. Considering a coefficient of variation, CV, as a measure of the gas-flow uniformity in the cross-sections of the ESP [2]:

$$CV = \frac{S_{\text{tdev}}}{v_{\text{ave}}} = \frac{1}{v_{\text{ave}}} \sqrt{\frac{\sum_{i=1}^{n} \left(v_i - v_{\text{ave}} \right)^2}{n-1}} \tag{1}$$

* Corresponding author, e-mail: zoda_mark@vin.bg.ac.rs

where $v_{ave} = 1/n \sum_{i=1}^{n} v_i$ [ms^{-1}] is the average gas velocity in the ESP cross-section, n – the number of velocity samples v_i, than Matts-Ohnfeldt generalized form of the ordinary Deutsch-Anderson equation of the ESP collection efficiency η could be written in the form [3]:

$$\eta \approx 1 - \mathrm{e}^{\left[-\left(\omega_k \left(1-k(CV)^2\right)^{\frac{1}{k}} \frac{A}{Q}\right)^k\right]} \tag{2}$$

where Q [m^{3}s^{-1}] is the gas-flow rate, ω_k [ms^{-1}] – the particle migration velocity, and A [m^2] – the ESP collecting electrode area. The parameter k [–] allows to compensate for different particle size distribution, usually having the value around 0.5 for coal-fired boilers, while $k = 1$ corresponds to uniform particle size distribution, thus to the original Deutch equation. The eq. (2) indicates that maximum theoretical ESP collection efficiency results from perfectly uniform gas velocity distribution over the ESP's chamber cross-section ($CV = 0$). This study aims to investigate flue gas-flow distribution inside the chamber and ductwork of ESP of 324 MWe lignite fired Unit A4 of the TPP *Nikola Tesla* in Obrenovac, Serbia. The main objective was to develop an optimized design of the guide vanes that will improve velocities distribution inside the ESP chamber. Since velocity profile varies significantly in vertical and transverse directions of the ESP vertical cross-sections, the dimensionless momentum M_k (Boussinesq coefficient) and energy correction coefficient N_k (Coriolis coefficient) were used to evaluate homogeneity [4]:

$$M_k = \frac{\int v^2 \mathrm{d}A}{v_{avg}^2 A_{tot}} = \frac{1}{A_{tot}} \sum_{i=1}^{n} \left(\frac{v_i}{v_{avg}}\right)^2 \Delta A_i, \quad N_k = \frac{\int v^3 \mathrm{d}A}{v_{avg}^3 A_{tot}} = \frac{1}{A_{tot}} \sum_{i=1}^{n} \left(\frac{v_i}{v_{avg}}\right)^2 \Delta A_i \tag{3}$$

where v_i [ms^{-1}] is the mean velocity through the elementary surface i of the cross-section of the ESP chamber, v_{avg} [ms^{-1}] – the mean velocity in the cross-section, ΔA_i [m^2] – the elementary surface and n – the number of elementary surfaces i in the cross-section of the ESP chamber. The values of M_k and N_k are equal to unity only under the uniform flow conditions. The further the flow deviates from uniformity, the greater these values become. According to guideline [5] the gas-flow homogeneity before the first ESP field could be considered as relatively good if 75% of the velocities are ≤ 1.15 times the mean gas velocity v_{avg}, with $CV < 0.25$ before the first electrical field and $CV \leq 0.2$ at the beginning of the subsequent fields. The guideline [6] criterion is often interpreted by qualifying the uniformity of the flow field when $CV \leq 0.15$ which results if a Gaussian distribution of velocities around the mean is assumed. It should be noted that gas velocities v_i, $i = 1, \ldots, n$ used in eq. (1) are supposed to be evaluated at the centres of the rectangles of the equal areas A_i that cross-section is divided into. In other cases, the L1 norm based metric of flow uniformity [7] is used:

$$\gamma_{L1} = 1 - \frac{1}{2}\left(\sum_{i=1}^{n} \frac{A_i}{A_{tot}} \frac{\left|v_i - v_{avg}\right|}{v_{avg}}\right) \tag{4}$$

where n is the number of the cross-section division, i – the cell index, A_i [m^2] – the face area of the cell, v_i – the component of velocity normal to the cell, tot – the total, and avg – the area-weighted average. For a perfectly uniform flow $\gamma_{L1} = 1.0$. Since velocity distributions in ESP may follow non-Gaussian distribution including skewed and multi-modal shapes, the L2 norm based measure of homogeneity [1] is also evaluated in this work:

$$\gamma_{L2} = 1 - \frac{1}{2v_{avg}}\left[\sqrt{\sum_{i=1}^{n} \frac{A_i}{A_{tot}} \left(v_i - v_{avg}\right)^2}\right] \tag{5}$$

For a perfectly uniform flow $\gamma_{L2} = 1.0$. In recent years the advance in the computer technology and numerical techniques allowed application of CFD in flow characteristics examination [8] and even performance optimization of different flow control devices [9]. The need for simplification of the complex full-scale geometry of ESP resulted in using the model of porous media of finite thickness with directional permeability for modelling the flow through the perforated plates [10]. The design of experiments by using Taguchi approach was implemented for optimization of the perforated plates over different parameters [9]. Yet, whenever was possible, as detailed as possible full-scale CFD modelling of the entire flow domain was applied [11] since noticeable deviation was reported between numerically calculated and measured velocity distribution [12]. Completely uniform flow throughout the cross-sections of the ESP chamber is neither achievable nor desired [6] due to the inevitable formation of low speed regions in the chamber. The highest dedusting performance of ESP requires a well-balanced flow distribution through the precipitation zones, imposing the necessary application of different flow control devices. Properly designed turning vanes assist the air-flow in making a smoother change in flow direction [13] resulting in less force transferred and noise generated [14] thus less pressure drop. As gas velocity increases, this effect becomes more pronounced. The flow pattern in the flue gas channels and chambers of Unit A4 were determined by measurements. A series of 22 detailed full-scale numerical models of ESP with guide vanes of different designs were simulated by using CFD. Flow uniformity was evaluated for selected vertical cross-sections of the ESP by calculating homogeneity parameters according to eqs. (1)-(5). For the purpose of testing against the requirements [6, 7] additional parameters were calculated: $A_{<85\%}$, $A_{>115\%}$ and $A_{>140\%}$ as per cent of total area of the cross-section that exhibit velocities < 85%, > 115% and >140% of v_{ave}, respectively. A guide vanes configuration which enabled the best homogeneity parameters, as lower as possible pressure drop through the ESP and overall weight of design, was selected for implementation. The results of velocity measurements after reconstruction of the ESP according to proposed design confirmed better flow uniformity in the ESP chamber compared to the original one. The results of measurements of particulate matter emission before [15] and after [16] reconstruction of the ESP according to proposed design confirmed decrease in emission. The novelty of this study is to develop new 3-D CFD models of a full-scale ESP taking into account its major physical features (collecting electrodes, guide vanes, perforated plates*, etc.*).

Geometry of the electrostatic precipitator of Unit A4

The dedusting system of the Unit A4 consist of two separate, plate-type, rigid-frame, dry ESP with eight dust collecting hoppers as shown on fig. 1. The ESP of type 2XEKE2-52/12/2x12-6/250 was built by ZVVZ – Milevsko under the license of Lurgi and reconstructed during the capital overhaul in 2007, by the consortium of RAFAKO S.A, ELWO S.A, Energoprojekt – Oprema and Energoprojekt – Entel. At the rotational air heater exit, flue gas is carried through the 2.5 m × 10.5 m horizontal channel hawing eight openings on the channel top wall for flue gas velocity measurements (the cross-section A-A, fig. 1). The flue gas channel is then bent upward through the 90° inlet elbow (pos. 1) into 3.2 m × 10.5 m inlet duct narrowed to 2.9 m × 9.1 m cross-section (pos. 2). At the top of vertical channel, flow 90° bents in to the pyramidal wide-angle diffuser (pos. 3) with 10.1 m × 9.1 m inlet cross-section, 2.5 m length and area ratio of 2.7 having divergence angles of 55° horizontally and 47° vertically. Six turning vanes, (pos. 4), detailed given on fig. 2(a), are placed in vertical channel at the inlet of diffuser for adequate flue gas distribution on the distribution grates. The first distribution grate (pos. 5) located in the inlet of diffuser, consists of 8 rows, each with 12 perforated plates of the porosity 0.48. The second distribution grate (pos. 6) consists of 12 rows with 18 perforat-

ed plates of the porosity 0.48, except for the plates next to the wall and 8 central plates in the fifth row which are of the porosity 0.36, and 6 central plates in the fourth row and 8 central plates in the sixth row which are of the porosity 0.42. The porosity of the plate is realized by 80 mm × 50 mm rectangular openings in adequate quadrilateral pitch. The ESP chamber is 17.6 m × 16.2 m× 15.4 m of the effective length, width and height, respectively, containing separately energized sections electrically divided into four electrical zones I-IV. Each electrical zone contains 40 collection electrodes (CE) of 3.4 m × 16.3 m forming 400 mm wide passages between neighbouring CE. The total area of CE is 23296 m^2 per chamber. The flue gas leaves the ESP chamber (pos. 7) through the 4 m long pyramidal wide-angle confusor (pos. 8) with divergence angles of 51° horizontally and 54° vertically, confusor area ratio of 9.2. One outlet distribution grate (pos. 9) of the porosity 0.6 is placed in the confusor. Through the 90° outlet elbow (pos. 10) and outlet channel (pos. 11) of 6.3 m × 4.0 m cross-section, the gas is conducted to the flue gas fan (FGF).

Numerical method

Investigation of the flow characteristics of ESP models with different guide vane configurations was based on the CFD simulation data at the cross-section of interest. The flow was considered a 3-D, single phase, steady-state, incompressible and isothermal. The CFD software package ANSYS-CFX was used for finite element-based finite volume discretization of spatial domain and for numerically solving the conservation equations for mass, momentum and additional two transport equations of the k-ε turbulence model. A coupled solver and fully implicit discretization of the hydrodynamic equations as a single system were applied. The high resolution advection discretization scheme was used for the calculation of variables at the mesh nodes and finite-element shape functions for value approximation at integration points. An independent multidomain step control partitioning, RMS solver residual type and 10^{-4} residual target value were assigned. The number of iterations and CPU simulation time until the convergence on AMD 2.2 GHz 4 GB RAM computing system varied between 80-350 iteration and 4-38 hours, respectively depending on the model solved. Due to axial vertical plane symmetry, a simplified full-scale CFD numerical model of one-half of the ESP chamber, inlet and outlet flue gas channels, accounting for guide vanes, distribution grates and CE was considered, but neglecting emission electrodes, small structural and joining elements. Models complexity imposed a hybrid numerical grid with a number of nodes that varied from around 230000 up to limitations for our computing resources of around 462000, depending on the model geometry. The numerical grid quality for each of the models was confirmed by checking the parameters of the mesh orthogonality, mesh expansion and mesh aspect ratio, as well as shapes of the residuals convergence curves. A general intersection algorithm with an automatic surface trimming function was used for surface treatment of the numerical fluxes across up to 8400 non-overlapped grid interfaces. The property of the modeled fluid on the working condition (temperature T = 170 °C and reference pressure p = 101325 Pa) was: density ρ = 0.774 kg/m^3, molar mass M = 29.1 kg/kmol, specific heat capacity under constant pressure c = 1097 J/kgK, dynamic viscosity v = 2.2511·10^{-5} Pa·s. The nominal flow of the wet flue gas on working condition through one ESP chamber is 1458000 m^3 per hour. Therefore, the inlet boundary condition was set at cross-section A-A containing the origin, fig. 1, with a uniform x-component of velocity u = 15 m/s allowing for the mass-flow rate of 304.8 kg/s over the whole cross-section of the inlet channel. The outlet boundary condition was set at the end of the outlet channel as static pressure of 0 Pa averaged over entire outlet cross-section.

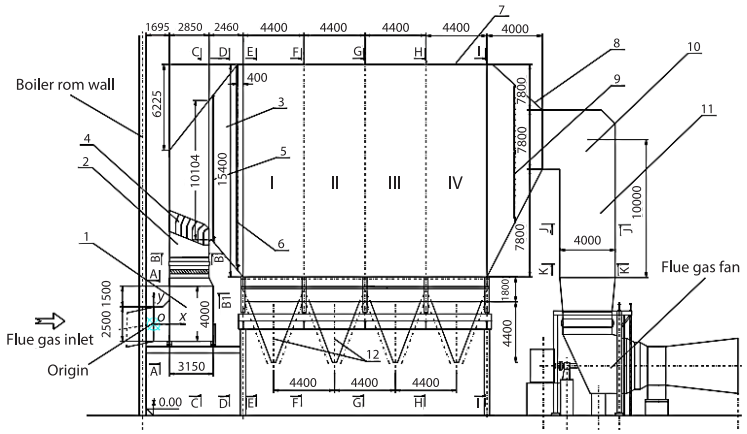

Figure 1. The ESP of 324 MWe lignit fired Unit A4 – vertical axial cross-section: *1 – inlet elbow, 2 – vertical channel, 3 – ESP diffuser, 4 – guide vanes, 5 – first distribution grate, 6 – second distribution grate, 7 – ESP chamber, 8 – confusor, 9 – outlet screen, 10 – outlet elbow, 11– outlet channel, 12 – hoppers, and I-IV – electrical zones;* **position of the cross-sections: A-A: x = 0 m; B-B: y = 5.5 m; C-C: x = 4.1 m; D-D: x = 5.5 m; E-E: x = 7 m; F-F: x = 11 m; G-G: x = 15.4 m; H-H: x = 19.7 m; I-I: x = 23.7 m; J-J: y = 5 m**

Symmetrical boundary conditions were used in vertical symmetry plane of ESP to ease the computational load. The walls, distribution grates, CE and the guide vanes were modelled as smooth solid walls. Scalable turbulent wall functions were applied for near-wall treatment purposes.

Results and discussion

Results of initial velocity measurements

In order to assess the flow pattern inside ESP with original turning vanes set, fig. 2(a) two series of air velocity measurements were performed with the boiler out of operation and FGF in operation, the adjusted current of the FGF electric motor of 152 A and opening of the FGF flaps of 11%. The air velocity profile in the horizontal flue gas ducts behind the air heater

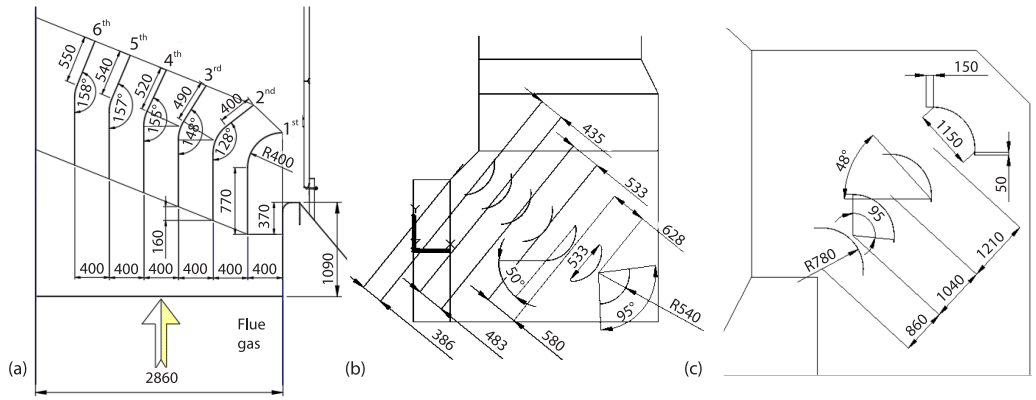

Figure 2. (a) The original design of guide vanes in diffuser (fig. 1 pos. 4), (b) proposed design of the guide vanes set in the inlet elbow, and (c) proposed design of the guide vanes set in the outlet elbow

in the cross-section A-A was determined by measurements at four measuring points per each of eight vertical axes distributed over the width of the channel according to the ISO 10780:1994 recommendations. Standard Pitot-Prandtl probe and Alnor AXD560 micromanometer with accuracy of ±2% of measured value were used for differential and static pressure measurements. Air temperature was measured by using PCE T 390 TC digital thermometer and *K*-type thermocouple with accuracy of ±1.2 °C. Results of measurements of the velocity component normal to the cross-section of flue gas channels are presented in fig. 3 in the form of contour plots over interpolated measuring data. Significant flow non-uniformity reflected in higher velocities near to side and top walls of the channels was confirmed. The minimal/average/maximal velocity was 6.8/8.6/10.8 m/s and 7.1/8.7/10.3 m/s with standard deviation of 1 m/s and 0.8 m/s for the left and right horizontal duct, respectively.

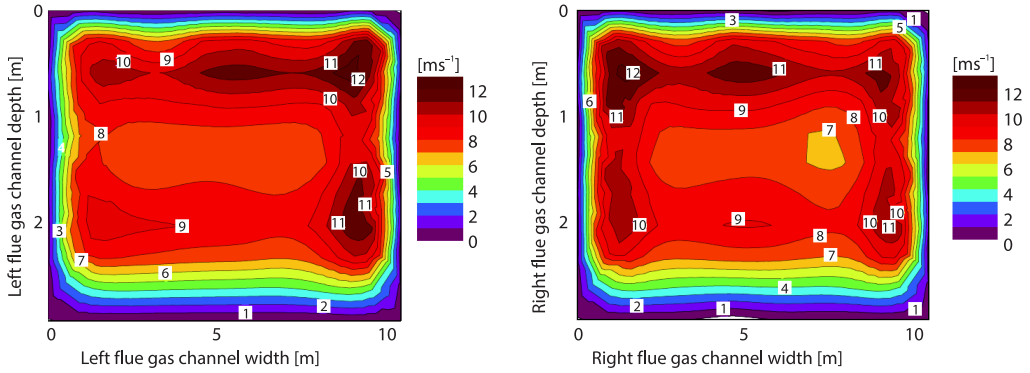

Figure 3. Air velocity distribution in the horizontal channels, measuring cross-sections A-A

The second series of velocity measurements were performed inside the right ESP chamber in the front of the 1st electrical field (cross-section E-E). A vane type anemometer Testo 435-4 with Ø100 mm vane as well as Testo 400 tip 0563 9501 with Ø100 mm vane was used. The anemometers were calibrated in a wind tunnel with the accuracy of the calibration of 1% or 0.05 m/s (whichever is greater). Air velocity was measured in 19 measuring points along the casing width at heights of 0 m, 1 m, 2 m, and 3.5 m from the internal walking platform, fig. 4(a), as well as in 12 measuring points along vertical lines 1.2 m left and right from the vertical ladder, fig. 4(b). Unfortunately, the ladder was blocked at the position of 10.5 m from the ESP door and was not able to be moved left-right along the width of the ESP chamber. Therefore, only a limited number of measurements along the ESP height were possible. Based on the mean of velocities measured in the channels (8.75 m/s) and the ratio of the areas of the cross-section of channels (10.5 m × 2.5 m) and the cross-section E-E (16.3 m × 15.6 m), the calculated mean velocity in the cross-section E-E was 0.9 m/s. Below 4 m in height over the entire cross-section E-E practically there is no flow since velocity was less than 0.3 m/s except in the vicinity of the walls, fig. 4(a). Above the height of 4 m the velocity field is uneven in the range of 1-3 m/s with two zones of velocities higher than 2.5 m/s, the one around the height of 5 m and the other extends from 8 m up to 13 m of the ESP height, fig. 4(b).

Both sets of results presented in fig. 4 clearly express the velocity field non-uniformity which deteriorates the dedusting efficiency of ESP both in the zones of low as well as in the zones of high flue gas velocities. Flow misdistribution is induced as early as in the front of the inlet elbow and the existing turning plates configuration is not able to improve the uniformity of flow through the diffuser and both distribution grates up to the first electrical field.

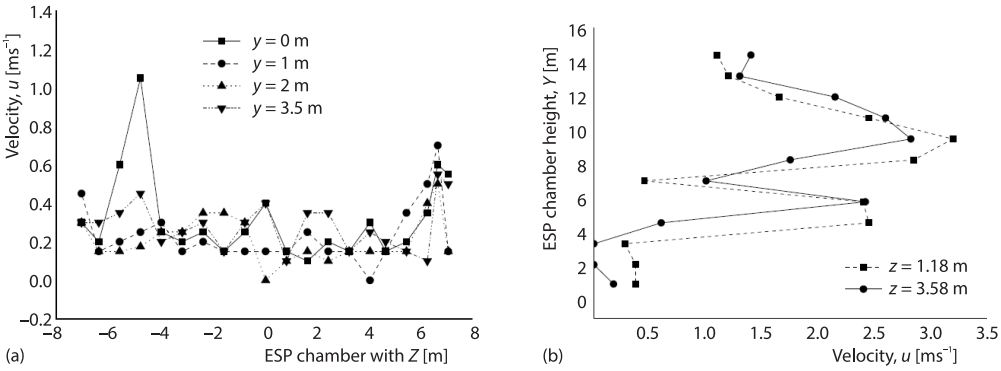

Figure 4. Results of measurements of the air velocity distribution in the right ESP chamber, measuring cross-section E-E; (a) along the ESP with on the heights of 0 m, 1 m, 2 m, and 3.5 m above the internal walking platform and (b) 1.2 m left and right along the vertical ladder

Results of the CFD numerical simulations

A series of 22 numerical simulations of ESP models with designs of guide vanes different in number, disposition and geometry characteristics were conducted. The configuration of the guide vane design and mass of the guide vane set and supporting structure are presented in tab. 1. The number of guide vanes set in the diffuser is denoted as N, while the number of guide vanes in the inlet and outlet elbow is denoted as N_1 and N_2, respectively. The disposition of the guide vanes sets and cross-sections of interest is presented on fig. 5(a). The geometric characteristics of the guide vanes in the diffuser presented on fig. 5(b) are: d [mm] is the thickness of the vane plate, l_1 [mm] is the upstream penetration, l_2 [mm] is the downstream penetration, α [°] is the angle of curvature, r [mm] is the radius of curvature, h [mm] is the distance between neighbouring centres of curvatures, β [°] is the inclination of guide vane set, t [mm] is the cord line extension, γ [°] is the angle between upstream penetration and the cord line, and δ [°] is the cord line inclination the normal.

Table 1. The guide vane design configuration

Case	1	2	3	4	5	6	7	8	9	10	11	12	13	14	15	16	17	18	19	20	21	22
N	6	6	6	6	6	6	6	8	8	10	10	10	10	12	12	12	12	12	13	13	14	20
N1	0	7	7	7	7	7	7	7	7	7	7	7	7	7	7	7	7	7	7	7	7	7
N2	0	0	0	4	4	4	4	0	4	4	4	4	4	0	0	0	0	0	4	4	0	0
m (t)	10.2	10.2	12.7	10.4	9.72	9.72	9.72	12.1	12.1	13.8	13.8	13.8	13.8	17.0	17.0	17.0	12.9	17.0	13.3	16.4	13.6	17.2
m_1 (t)	0.0	11.2	11.2	11.2	11.2	11.2	11.2	11.2	11.2	11.2	11.2	11.2	11.2	11.2	11.2	11.2	11.2	11.2	11.2	11.2	11.2	11.2
m_2 (t)	0.0	0.0	0.0	5.2	5.2	5.2	5.2	0.0	5.2	5.2	5.2	5.2	5.2	0.0	0.0	0.0	0.0	0.0	5.2	5.2	0.0	0.0

The values of geometric parameters for designs of guide vanes in the diffuser defining numerical Cases 1-22 are presented in tab. 2. The first value in the tab. 2 cells corresponds to the bottom turning vane in the set, the next value corresponds to the upper turning vane and so on. If cell contain only one value, this value is applied for all vanes in the series. The geometric parameters, fig. 5(b) of the original design of turning vanes in the diffuser are presented on fig. 2(a) and given in the first row of the tab. 2, denominated as Case 1. The thickness of the 1st (lowest) vane is d = 6 mm, the upstream penetration l_1 = 770 mm, downstream penetration l_2 = 0 mm, angle of the vane curvature α = 90°, radius of the vane curvature r = 400 mm, the

distance between neighbouring centres of curvatures h = 516 mm, the inclination of guide vane set β = 68°, the cord line extension of the vane t = 566 mm, the angle between upstream penetration and the cord line γ = 45 °, inclination the normal of the vane's cord line δ = 45 °. Accordingly, for the 2nd guide vane, the geometric parameters are: d = 6 mm, l_1 = 770 mm, l_2 = 400 mm, α = 52 °, r = 400 mm, h = 431 mm, β = 68°, t = 351 mm, γ = 26°, and δ = 26 °. The geometric parameters of the guide vane sets in the inlet and outlet elbow are presented on figs. 2(b) and 2(c), respectively.

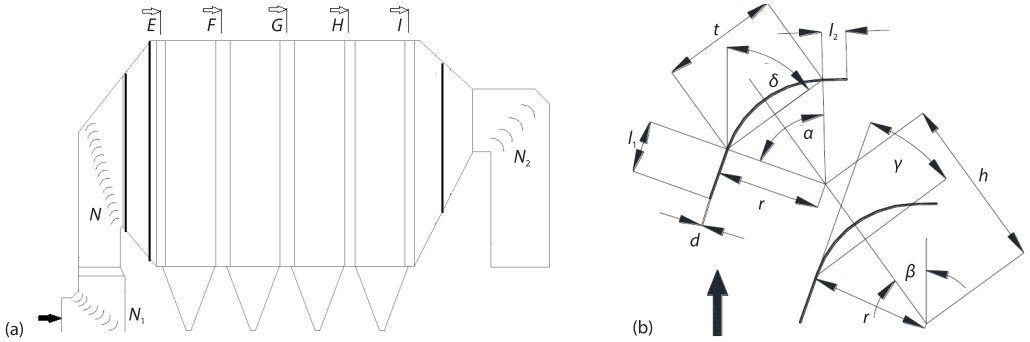

Figure 5. Disposition of the guide vanes set (a) and geometric characteristics of the guide vanes in the diffuser (b)

The numerical model of ESP with original design of guide vanes, fig. 2(a) is denoted as Case 1. The results of numerical simulation for model Case 1 are presented in the form of contour plots of u-velocity component in the cross-section E-E before the 1st electrical field, fig. 6(a) and in the cross-section I-I behind the 4th electrical field, fig. 6(b). Velocity magnitude is numbered on contour plot presented on one-half of ESP cross-section where z-co-ordinates corresponds to the ESP chamber width and y-co-ordinates to the chamber height. Numerical simulation of model Case 1 predicts flow separation in the inlet elbow and increased boundary-layer on the channel wall toward the boiler room. Guide vanes of the original design are not able to straightener and turn such unsymmetrical flow from the vertical channel to the outlet of diffuser therefore, flow impacts distribution grates with low perpendicular and high tangential component of velocity.

This results in higher velocities (>1.4u_{ave}, u_{ave} = 1.5 m/s) near the ceiling and side walls of the ESP chamber and low velocities in the central and bottom part of the cross-section E-E, fig. 6(a). The sucking effect of the confusor outlet induce higher velocities near the ESP ceiling leaving lower half of I-I cross-section practically with no flow, fig. 6(b). Calculated flow uniformity parameters are very poor in all vertical cross-sections along the ESP (M_k > 2.35, γ_{L1} < 0.50 and γ_{L2} < 0.42) while parameters $A_{<85\%}$ and $A_{>115\%}$ are greater than 40% and 30%, respectively. Therefore, neither uniformity criterions (1)-(5) are fulfilled or [5, 6] compliance satisfied.

The series of additional 21 numerical simulations of ESP models with different concepts of turning vane designs were conducted and results of simulations are compared. Tested concepts differ in turning vanes configurations, tab. 1, numbers and geometric parameters of the guide vanes in the diffuser, tab. 2. The parameters M_k and N_k calculated on the results of the simulations for the cross-section E-E as well as values of pressure drop dP [Pa] and overall weight m_{tot} [ton] of applied guide vane design concept (including mass of supporting structure) are presented on fig. 7. A set of 7 turning vanes in inlet elbow, fig. 2(b) denoted as N_1 is defined

Table 2. The geometric parameters of tested designs of the guide vanes in the diffuser

Case	d [mm]	l_1 [mm]	l_2 [mm]	α [°]	r [mm]	h [mm]	β [°]	t [mm]	γ [°]	δ [°]
1	6	770	0; 400; 490; 520; 540; 550	90; 52; 32; 25; 23; 22	400	516; 431; 431; 431; 431; 431	68	566; 351; 221; 173; 159; 153	45; 26; 16; 13; 11	45; 26; 16; 13; 11
2	6	770	0; 400; 490; 520; 540; 550	90; 52 32; 25 23; 22	400	516; 431; 431; 431; 431; 431	68	566; 351; 221; 173; 159; 153	45; 26; 16; 13; 11	45; 26; 16; 13; 11
3	5	770	0; 0; 270; 360; 390; 450	90; 90 52; 47 40; 37	400	516; 893; 893; 893; 893; 893	29	566; 566; 351; 300; 274; 254	45; 45; 26; 22; 20; 19	45; 45; 26; 22; 20; 20
4	6	450; 100; 60; 60; 60; 60	40	95	360; 460; 540; 540; 540; 540	480; 608; 726; 1040; 996; 1012	25	530; 680; 800; 800; 800; 800	48	55; 55; 55; 55; 57; 57
5	5	450; 100; 100; 100; 100; 100	40	95	360; 460; 540; 540; 540; 540	459; 861; 973; 1377; 1377; 1360	18	530; 680; 800; 800; 800; 800	59, 48, 48, 48, 48, 48	59; 57; 57; 55; 53; 53
6	5	450; 100; 100; 100; 100; 100	40	95	360; 460; 540; 540; 540; 540	458; 858; 972; 1374; 1373; 1360	18	530; 680; 800; 800; 800; 800	59; 48; 48; 48; 48; 48	60
7	5	450; 100; 100; 100; 100; 100	40	95	360; 460; 540; 540; 540; 540	458; 858; 972; 1374; 1373; 1360	18	530; 680; 800; 800; 800; 800	59; 48; 48; 48; 48; 49	60
8	5	250; 250; 250; 200; 55; 55; 200; 235	50; 50; 50; 50; 0; 0; 50; 50	95	362; 374; 437; 514; 570; 570; 511; 414	375; 614; 634; 697; 752; 863; 950; 1047	35	533; 552; 644; 758; 840; 840; 754; 611	48	55
9	5	250; 250; 250; 200; 55; 55; 200; 235	50; 50; 50; 50; 0; 0; 50; 50	95	362; 374; 437; 514; 570; 570; 511; 414	370; 614; 634; 697; 752; 863; 950; 1047	23	533; 552; 644; 758; 840; 840; 754; 611	48	55
10	5	200; 200; 200; 200; 200; 100; 100; 100; 100; 100	0; 0; 0; 0; 0; 0; 0; 0; 0; 100	95	483; 483; 483; 483; 483; 540; 540; 540; 540; 540	541; 586; 631; 676; 721; 766; 811; 856; 900; 775	17	712; 712; 712; 712; 712; 800; 800; 800; 800; 800	55; 47; 47; 47; 47; 48; 48; 48; 48; 48	55
11	5	200; 200; 200; 200; 200; 100; 100; 100; 100; 0	0	95	483; 483; 483; 483; 483; 540; 540; 540; 540; 540	541; 580; 629; 670; 708; 744; 812; 857; 900; 837	17	712; 712; 712; 712; 712; 800; 800; 800; 800; 800	55; 47; 47; 47; 47; 48; 48; 48; 48; 48	55
12	5	200; 200; 200; 200; 200; 100; 100; 100; 100; 100	0	95	483; 483; 483; 483; 483; 540; 540; 540; 540; 540	541; 580; 629; 675; 708; 734; 812; 857; 906; 827	17	712; 712; 712; 712; 712; 800; 800; 800; 800; 800	55; 47; 47; 47; 47; 48; 48; 48; 48; 48	55; 55; 55; 55; 55; 60; 60; 60; 60; 60

→

Table 2. Continuation

Case	d [mm]	l_1 [mm]	l_2 [mm]	α [°]	r [mm]	h [mm]	β [°]	t [mm]	γ [°]	δ [°]
13	5	200; 200; 200; 200; 200; 100; 100; 100; 100; 100	0	95	483; 483; 483; 483; 483; 540; 540; 540; 540; 540	541; 580; 629; 675; 712; 743; 812; 857; 900; 827	17	712; 712; 712; 712; 712; 800; 800; 800; 800; 800	55; 47; 47; 47; 47; 48; 48; 48; 48; 48	60
14	6	0	0	95	678	323; 470; 498; 528; 557; 586; 615; 642; 674; 703; 732; 762	11	1000	48	55
15	6	0	0	95	678	440; 470; 498; 528; 557; 586; 615; 642; 674; 703; 732; 550	11	1000	47	75
16	6	0	0	95	678	440; 470; 498; 528; 557; 586; 615; 642; 674; 703; 732; 762	11	1000	48	59
17	6	0	0	95	570	554; 470; 498; 528; 557; 586; 615; 642; 674; 703; 732; 762	11	840	47	59; 59; 59; 59; 59; 57; 55; 55; 55; 55; 55; 55; 55; 55
18	6	0	0	95	678	440; 470; 498; 528; 557; 586; 615; 642; 674; 703; 732; 762	11	1000	47	59; 59; 59; 59; 59; 55; 55; 55; 55; 55; 55; 55; 55; 55
19	5	0	0	95	483; 483; 483; 483; 483; 570; 570; 570; 570; 570; 570; 570; 570; 570	323; 554; 554; 554; 554; 517; 568; 550; 550; 550; 550; 550; 550; 550	15	712; 712; 712; 712; 712; 840; 840; 840; 840; 840; 840; 840; 840; 840	48	59; 59; 59; 59; 59; 57; 55; 55; 55; 55; 55; 55; 55; 55
20	6	0	0	95	483; 483; 483; 483; 483; 570; 570; 570; 570; 570; 570; 570; 570; 570	554	15	712; 712; 712; 712; 712; 840; 840; 840; 840; 840; 840; 840; 840; 840	48	55
21	5	0	0	95; 95; 95; 95; 95; 95; 95; 95; 95; 95; 95; 95; 95; 95; 40	482; 482; 482; 482; 482; 570; 570; 570; 570; 570; 570; 570; 570; 570	320; 554; 554; 554; 554; 493; 580; 550; 550; 550; 550; 550; 550; 373	15	710; 710; 710; 710; 710; 840; 840; 840; 840; 840; 840; 840; 840; 394	48	59; 59; 59; 59; 59; 57; 55; 55; 55; 55; 55; 55; 55; 55
22	6	0	0	95	362	368	19	533	47	55

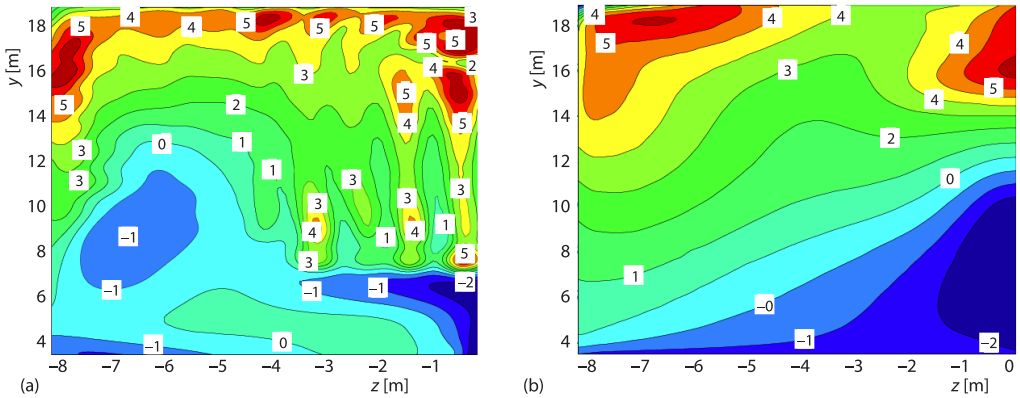

Figure 6. Numerical model Case 1, *u* [m/s] component of the flue gas velocity distribution before the 1st (a) and behind the 4th electrical field (b) of one half of the ESP chamber (at $z = 0$ is the axial symmetry plain)

according to literature recommendation [17] for a given geometry of the 90° inlet elbow and introduced into numerical models of ESP in order to improve flow uniformity in vertical channel (pos.2). The effectiveness of set of vanes N_1 reflects in improvements of the homogeneity parameters in the cross-section B-B (for all cases 2-22): $CV < 15\%$, $M_k \sim 1.0$, $\gamma_{L1} > 0.95$ and $\gamma_{L2} < 0.94$, $A_{<85\%} < 15\%$ and $A_{>115\%} = A_{>140\%} = 0\%$, but also in the cross-section E-E since values of the calculated parameters M_k and N_k reduced from 2.35 and 5.37 for the Case 1 to the values of 2.01 and 4.56 for the Case 2, respectively, fig. 7. The set of four turning vanes in outlet elbow, fig. 2(c) denoted as N_2 is introduced in some models in order to improve flow uniformity in the outlet channel (pos.11), to reduce pressure drop through the outlet elbow, but also to improve uniformity in the cross-section I-I. Effectiveness of this set of vanes on the flow uniformity is positive but of a lesser degree comparing the influence of the guide vanes set N_1. Parameters M_k and N_k, calculated as 1.49 and 2.96, respectively for the cross-section E-E of model Case 8 (without the set N_2), are only 7% and 36% higher than values of 1.40 and 2.17, calculated as parameters M_k and N_k for the cross-section E-E of the model Case 9 which contains set N_2, fig. 7. Also, the pressure drop reduced around 4% from 319 Pa in the model Case 8 to the 308 Pa in the model Case 9. Numerical models with $N = 6$ turning vanes in the diffuser of different geometric characteristics (Cases 3-7) were tested in attempt to establish as uniform as possible flow by using the same number of vanes as existing one and to keep the overall weight of the vanes and supporting structure as lighter as possible. The best results has been achieved with model Case 4 with parameters M_k and N_k calculated for the cross-section E-E of 1.40 and 2.16, respectively, while $dP = 300$ Pa , fig. 7, but neither uniformity criterions are fulfilled nor [5] or [6] compliance satisfied. Therefore, additional numerical models of ESP Cases 8-22 with a greater number of blades in the diffuser were tested, tab. 1.

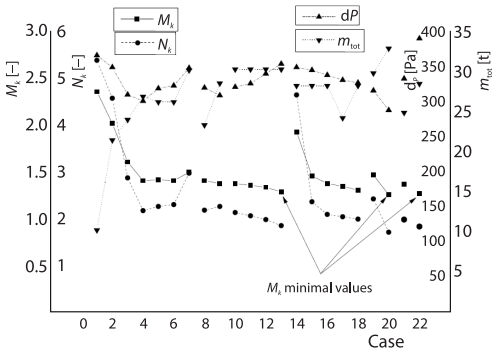

Figure 7. Parameters M_k, N_k for the cross-section E-E and pressure drop dP calculated based on results of numerical simulations; overall weight of the guide vanes design applied in the model

Generally, increasing the number of vanes N improved flow homogeneity resulting in decrease of parameters M_k and N_k calculated for the cross-section E-E, but also increase the pressure drop dP and overall weight of the design m_{tot} , fig. 7. In addition the numerical models with set of 10, 12, and 13 guide vanes in the diffuser defined according to literature data [17], models with guide vanes design of modified geometry and disposition comparing to theoretical one were considered. Modifications were based on the results of investigation of flow distribution in vertical cross-sections of ESP in order to avoid zones of inadequate velocity distribution near the walls and ceiling of ESP. Regarding the values of parameters M_k and N_k calculated for the cross-section E-E the best results are obtained for numerical models designated as Case 13, Case 20 and Case 22, fig. 7. The numerical model Case 22 with a set of 20 turning vanes in the diffuser is presented for the comparison purpose only due to the fact that practical construction and installation of this design cause significant practical problems. Additional disadvantages of this concept are the high weight of the set of vanes in the diffuser (17.2 tons) as well as the overall weight of the concept (28.4 tons), and also the high value of pressure drop (dP = 389 Pa). The uniformity parameters calculated based on the results of numerical simulations Case 13 and Case 20 for the selected cross-sections are presented in tab. 3. One concludes that in all cross-section of interest the vane design applied in Case 20 provide better flow uniformity, especially in the cross-section I-I (values of calculated CV, M_k and $A_{<115\%}$ in these two cases differs up to 26%, 13%, and 23%, respectively). Also, the calculated pressure drop dP for Case 20 is 287 Pa, much lower than the value of 353 Pa calculated for the Case 13. On the other hand, the values of parameters γ_{L1} and γ_{L2} calculated in the cross-sections of interest for these two cases differ only within the range of 10% throughout the whole ESP chamber. Furthermore, the value of the parameter $A_{<85\%}$ for the 2nd, 3th, and 4th electrical fields is more than 10%, while value of parameter $A_{<140\%}$ for the 1st electrical field is more than 13% larger for Case 20 comparing to Case 13, indicating that smaller areas of the cross-sections in the Case 13 exhibit velocities lower than $0.85u_{ave}$ and greater than $1.4u_{ave}$. Comparing the u-component of velocity distribution in all cross-sections of interest one see that the distribution provided by Case 13 is somehow more uniform than distribution provided by Case 20. Velocity distribution in the cross-sections E-E in Case 13, fig. 8(a) is smoother with fewer zones of much higher and much lower velocities than the average value of 1.5 m/s compared to Case 20, (fig. 8(b). The impact of sucking effect of confusor outlet on the velocity distribution in the cross-section I-I is lesser in the Case 13, fig. 8(c) comparing to the Case 20, fig. 8(d).

Table 3. Case 13 and Case 20 flow uniformity statistics

Param.	CV [%]		γ_{L1} [–]		γ_{L2} [–]		M_k [–]		$A_{<85\%}$ [%]		$A_{>115\%}$ [%]		$A_{>140\%}$ [%]	
Case	13	20	13	20	13	20	13	20	13	20	13	20	13	20
B-B	12.6	14.0	0.97	0.97	0.95	0.95	1.01	1.01	8.4	7.7	0.0	0.0	0.0	0.0
E-E	54.1	52.9	0.80	0.85	0.74	0.76	1.28	1.25	31.7	31.2	38.1	34.4	20.8	23.6
F-F	72.3	68.2	0.69	0.71	0.64	0.66	1.53	1.46	42.9	46.7	44.7	40.7	31.0	30.2
G-G	64.4	57.0	0.69	0.76	0.63	0.72	1.56	1.32	44.3	48.8	43.8	36.1	27.2	25.3
H-H	68.3	54.4	0.74	0.79	0.67	0.74	1.43	1.28	43.6	45.2	36.7	34.5	22.6	21.2
I-I	88.1	70.1	0.68	0.73	0.61	0.67	1.62	1.44	36.5	44.3	46.2	37.6	31.0	29.3

Taking into account that the overall weight of the Case 20 guide vanes design without vanes set in the outlet elbow is m_{tot} = 32.8 tons (9% higher than the overall weight of the guide vanes design in Case 13), the design of the guide vanes applied in the numerical model Case 13 was selected as most promising and proposed to be built into the flue gas ductwork of the Unit A4 ESP during the overhaul.

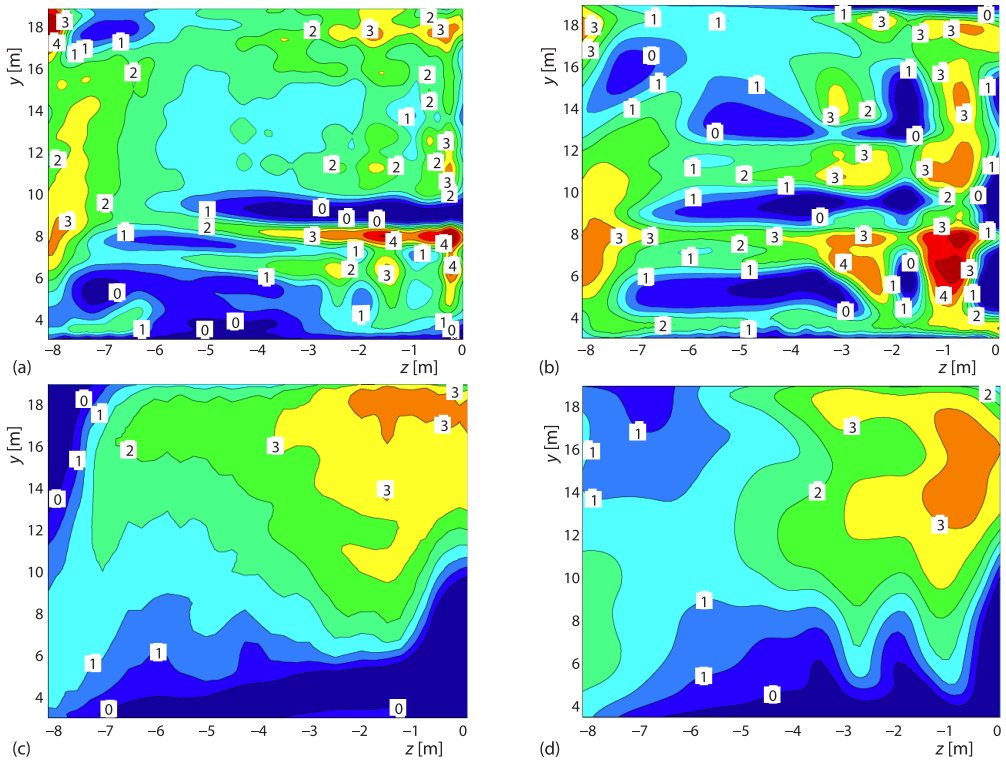

Figure 8. Contour plot of *u*-velocity [ms^{-1}] field in the cross-sections E-E (a) and (b) and I-I (c) and (d) for Case 13 (a) and (c) and Case 20 (b) and (d); *z* is co-ordinate along chamber width and *y* is co-ordinate along the height of the model of one half of the ESP chamber (at *z* = 0 is the axial symmetry plain)

Results of velocity measurements after installation of the proposed guide vanes concept

After reconstruction of turning vanes according to technical solution as defined in numerical model Case 13, measurements of air velocity distribution in the chambers of the ESP were made with boiler and ESP out of operation and FGF in operation. In the right and left ESP chamber the measurements were conducted along the chamber width in the cross-section E-E in the front of 1st electrical field, at heights of 1 m, 2 m, and 3.5 m above the internal platform, fig. 9(a). Also, in the cross-section E-E of the right ESP chamber the measurements were conducted along the ESP height, 1.2 m left and right along the vertical ladder, fig. 9(b) as well as along the chamber width in the cross-section I-I after the 4th electrical field, at heights of 1 m, 2 m, and 3.5 m above the internal platform, fig. 9(c).

Comparing results of the velocity measurements in ESP before, fig. 4 and after, fig. 9 reconstruction of guide vanes according to the proposed design denoted as Case 13, one can notice significant improvements in the flow distribution in the cross-section E-E, both along the width and height of the ESP. The measurements confirmed more uniform vertical velocity profiles, fig. 9(b), than before the reconstruction, fig. 4(b). The satisfactory flow was also achieved in the lower third of both right and left ESP chamber, fig. 9(a), where practically there was no flow before reconstruction, fig. 4(a). Also, measurements of the velocity distribution behind the

4th electric field indicate that there is a satisfactory level of flow even in the lower part of the chamber below 3.5 m, fig. 9(c). By integrating elementary flows along the cross-section E-E based on measured velocity distribution in the cross-section E-E, one calculates $v_{ave} = 0.93$ m/s, $M_k = 1.2$ and $N_k = 1.75$, corresponding to the requirement of $M_k \leq 1.2$ for the flow uniformity through the ESP of high dedusting efficiency [4]. Emission of PM before the ESP reconstruction [15] was determined as 70.6 mg/Nm^3, 67.6 mg/Nm^3 and 62.8 mg/Nm^3 by three consecutive measurements, respectively, performed by the accredited laboratory of Mining Institute Ltd., Belgrade according to the standards SRPS ISO 9096:2010 and SRPS EN 13284-1:2009.

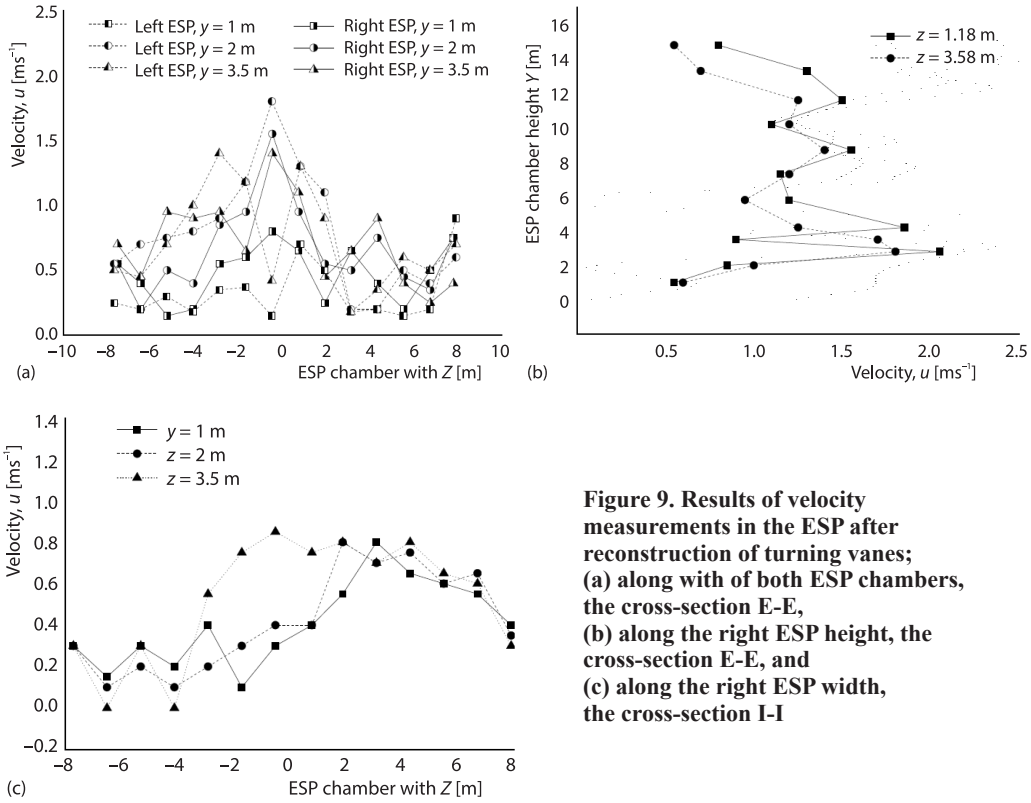

Figure 9. Results of velocity measurements in the ESP after reconstruction of turning vanes; (a) along with of both ESP chambers, the cross-section E-E, (b) along the right ESP height, the cross-section E-E, and (c) along the right ESP width, the cross-section I-I

After the reconstruction of the ESP according to the proposed guide vanes design, three consecutive measurements of PM emission were conducted by the same accredited laboratory according to standards SRPS ISO 9096:2019 and SRPS EN 13284-1:2017. The PM emission have been determined as 21.9 mg/Nm^3, 26.5 mg/Nm^3, and 25.8 mg/Nm^3, respectively [16]. Some basic parameters of the measurements conducted before and after the ESP reconstruction are presented in tab. 4. It should be emphasised that during the measurements conducted after the reconstruction of ESP, unit achieved up to 20% less power, with around 2% higher coal consumption and 6% lower flue gas-flow comparing to the measurements before reconstruction. The flue gas temperature and H_2O content were almost the same in both measurements.

Therefore, results of measurements presented in reports [15, 16] indicated that improvement of the velocity distribution in the chamber of the ESP of Unit A4 contributed to the reduction of PM emission from ESP.

Table 4. Unit A4 working parameters, flue gas characteristics and measured PM concentration in the flue gas as determined before [15] and after [16] reconstruction

		Before reconstruction (left/right flue gas channel)			After reconstruction (left/right flue gas channel)		
Measurement series		R1	R2	R3	R1	R2	R3
Unit	Power [MWe]	306.6	307.3	306.6	235.5	252.5	254.6
	Coal consumption [ton per hour]	412	400	415	396	420	425
	Flue gas-flow* [m^3 per hour]	1424700/ 1451700	1377900/ 1403100	1403100/ 1413900	1259100/ 1347300	1223100/ 1428300	1256400/ 1441800
Flue gas	O_2 content [vol.%]	7.2/7.3	7.3/7.2	7.2/7.1	7.5/7.0	7.5/7.6	7.5/7.7
	T [°C]	138/150	139/150	138/151	140/173	142/172	144/169
	H_2O content [vol.%]	21.3/21.1	21.2/21.3	21.2/21.2	22.9/23.6	23.2/23.0	23.1/21.7
PM concentration** [mgm^{-3}]		59.9/81.5	47.8/87.6	40.8/85.3	31.6/12.4	34.2/19.4	35.5/16.8

* on real condition in the flue gas channel, ** on standard condition 273.15 K; 101.3 kPa; dry gas; 6% O_2

Conclusion

This paper presents results of multi-parameter optimization of the design of turning vanes of the ESP of Unit A4 TPP *Nikola Tesla* in Obrenovac. The goal was to define as light as possible design that will enable the best flue gas-flow homogeneity in the ESP chamber with the lowest possible pressure drop through the ESP. The selection of the most favourable design was made based on the results of a series of 22 CFD numerical simulations of the flow through the ESP numerical models with different designs of turning vanes. The applied designs differ in concept (with or without guide vanes in the inlet and outlet elbow), the number and geometric characteristics of the guide vanes set in the diffuser. The significant influence of the set of guide vanes in the inlet elbow on the flow uniformity was proved. The positive influence of guide vanes in the outlet elbow on flow has been noticed also but with less degree compared to the level of influence of guide vanes in the inlet elbow. Generally, the greater number of blades in the diffuser provides better homogeneity of the flow through the ESP. The final solution has been selected among two concepts of 10 and 13 turning blades in the diffuser, having similar values of calculated homogeneity parameters, based on the result of further analysis of velocity distributions in the cross-sections of ESP. A new design concept was experimentally validated by measurements of the air velocities in the ESP chamber after the installation of the proposed guide vanes design. The measurements confirmed the improvement of the flow uniformity in the ESP chamber, both in the lower ESP zone and along the width and the height of the ESP compared to flow distribution in the ESP chamber before reconstruction. Based on the results of measurements of velocity distribution, the dimensionless correction coefficient M_k (Boussinesq coefficient) is calculated as 1.2, corresponding to the literature requirement [4] of $M_k \leq 1.2$ for the flow uniformity demands for ESP of high dedusting efficiency. This value correlates well to the value of $M_k = 1.28$ calculated from the results of the simulation of the corresponding numerical model. Measurements of the ESP particulate matter emission before and after the reconstruction of the guide vanes proved reduction of the emission from the average level of 67 mg/Nm^3 to the average level of 24.7 mg/Nm^3. This results indicate that improvement of the flue gas-flow field inside ESP chamber contributed to the particulate emission reduction.

Acknowledgment

The authors would like to acknowledge their high appreciation the Ministry of Education, Science and Technological Development of Republic of Serbia (Project No. III42010 *Reduction of Air Pollution from Thermal Power Plants of the PE Electric Power Industry of Serbia* and research theme *Improving the efficiency of equipment for waste gas purification and exploitation processes by increasing the fuel quality and assessing the impact on air pollution* which is being realized in *VINČA* Institute of Nuclear Sciences – National Institute of the Republic of Serbia, University of Belgrade, Belgrade, Serbia), as well as to Public Enterprise *Electric Power Industry of Serbia*, Belgrade, Serbia.

References

[1] Munnannur, A., *et al*., Development of Flow Uniformity Indices for Performance Evaluation of Aftertreatment Systems, *SAE Int. J. Engines*, *4* (2011), 1, pp. 1545-1555
[2] Dabiri, S., *et al*., Design of an Innovative Distributor to Improve Flow Uniformity Using Cylindrical Obstacles in Header of a Fuel Cell, *Energy*, *152* (2018), June, pp. 719-731
[3] Matts, S., Ohnfeldt, P. O., Efficiency Gas Cleaning With Sf Electrostatic Precipitators, *Flakten*, *1-2* (1963/64), pp. 93-110
[4] Zhou, J., *et al*., Energy and Momentum Correction Coefficients Within Contraction Zone in Open-Channel Combining Flows, *Water Science and Engineering*, *14* (2021), 4, pp. 337-344
[5] ***, VDI 3678 Part 1, Electrostatic precipitators – Process and waste gas cleaning, VDI/DIN-Handbuch Reinhaltung der Luft, Band 6: Abgasreinigung-Staubtechnik, Berlin: Beuth Verlag, 2011
[6] ***, Electrostatic Precipitator Gas-flow Model Studies, Publication ICAC-EP-7, Institute of Clean Air Companies, Washington, DC, USA, 2004
[7] Ngo, T. T., *et al*., Enhancement of Exit Flow Uniformity by Modifying the Shape of a Gas Torch to Obtain a Uniform Temperature Distribution on a Steel Plate During Preheating, *Applied Sciences*, *8* (2018), 11, 2197
[8] Bhasker, C., Flow Simulation in Electro-Static Precipitator (Esp) Ducts with Turning Vanes, *Adv. Eng. Softw*., *42* (2011), 7, pp. 501-512
[9] Celik, N., *et al*., Design Analysis of Fluid-Flow through Perforated Plates, *Thermal Science*, *22*, (2018), 6B, pp. 3091-3098
[10] Smierciew, K., *et al.*, Numerical Prediction of Homogeneity of Gas-flow through Perforated Plates, *Processes*, *9* (2021), 10, 1770
[11] Calautit, J. K., *et al*., A Validated Design Methodology for A Closed-Loop Subsonic Wind Tunnel, *Journal of Wind Engineering and Industrial Aerodynamics*, *125* (2014), Feb., pp. 180-194
[12] Haque, S. M. E., *et al*., Flow Simulation in an Electrostatic Precipitator of A Thermal Power Plant, *Applied Thermal Engineering*, *29* (2009), 10, pp. 2037-2042
[13] Hurtado, J. P., *et al*., Optimization Study of Guide Vanes for The Intake Fan-Duct Connection Using CFD, *Processes*, 9 (2021), 1555
[14] Rašuo, B., *et al*., A Study of Aerodynamic Noise in Air Duct Systems with Turning Vanes, *FME Transactions*, *49* (2020), 2, pp. 308-314
[15] ***, Test report no. E-28/16/JPEPS/TENT-A 456 Periodic Measurements of Pollutant Emissions into the Air at the TPP ‘’Nikola Tesla A” on Units A4, A5 and A6, Mining Institute Ltd. Belgrade, Serbia, 2016 (in Serbian)
[16] ***, Test report no. E-05/20/JPEPS/TENT-A 456 Periodic Measurements of Pollutant Emissions into the Air at the TPP "Nikola Tesla A" on Units A4, A5 and A6, Mining Institute Ltd. Belgrade, Serbia, 2020 (in Serbian)
[17] Idelchik, I. E., Handbook of Hydraulic Resistance, *Coefficients of Local Resistance and of Friction*, 3rd ed., Begell House, Inc., Danbury, Conn., USA, 1996

Paper submitted: September 3, 2022
Paper revised: December 8, 2022
Paper accepted: December 12, 2022